31 pp.

# A THERMAL VACUUM TECHNIQUE FOR MEASURING THE SOLAR ABSORPTANCE OF SATELLITE COATINGS AS A FUNCTION OF ANGLE OF INCIDENCE

Marla G. Hoke*

NASA GODDARD SPACE FLIGHT CENTER, Greenbelt, Md.

35221

An experimental technique for measuring the solar absorptance of a satellite coating as a function of angle of incidence has been developed. A thermal vacuum method is used to measure the equilibrium temperature of a coated sample as the sample is turned with respect to the incident beam by means of a rotational apparatus installed in the vacuum chamber. Preliminary measurements of the directional solar absorptance of the following materials have been made: evaporated aluminum, evaporated gold, aluminum leafing paint, zinc sulfide paint, and Parson's black paint. The hemispherical solar absorptance is calculated for evaporated aluminum.

Author



*Aerospace engineer, Coatings Section, Thermal Systems Branch.

# INTRODUCTION

A fundamental problem in the analysis and design of temperature controlled spacecraft is the prediction of the equilibrium temperature of the satellite in orbit. In order to solve the radiation balance equation for the equilibrium temperature of a satellite, the solar absorptances of the spacecraft surfaces are usually required. Due to the surface geometry of the satellite its surfaces usually do not lie perpendicular to the incident sun-illumination. Therefore, it is of fundamental importance to know the solar absorptance of a coating as a function of angle of incidence.

The average solar absorptance of a coating can be measured by knowing the equilibrium temperature of the sample coating when suspended in an evacuated chamber and illuminated by a source whose spectral distribution is similar to that of the sun. A rotating frame apparatus was designed which allows a sample, placed in the frame, to be turned to different angles with respect to the incident illumination. Since a gear coupling was employed to rotate the frame, a calibration technique, using the optical method of superposition of reflected and incident parallel beams, was devised in order to determine the true angular position of the sample.

Directional solar absorptances of the following materials have been measured: evaporated aluminum, evaporated gold, aluminum leafing paint, zinc sulfide paint, and Parson's black paint. Curves



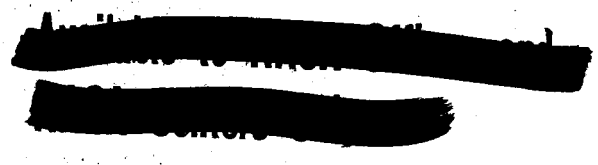

obtained from this data appear to agree well with theoretical expectations based on the Fresnel equations. The evaporated aluminum data was used to illustrate the calculation of the surface-average solar absorptance for a sphere.

## THE ROTATIONAL APPARATUS

### Design and Alignment of Sample Holders and Support Shafts

The apparatus designed for this experiment consists of two sample holders and the hardware necessary for adapting the system for installation through the existing vacuum system base plate.

The sample holders are 1/4 inch stainless steel rods welded into a trapezoid shape (Figure 1). Each frame is connected to its supporting shaft with a drift pin which permits removal of each frame while changing samples without disturbing the angular calibration. The upper frame, which remains in a fixed position in the vacuum chamber, houses the monitor sample, which monitors the relative intensity of the incident light. The lower frame houses the test sample; it rotates about a self-centering pivot point.

The test sample used with this experiment is a 1.5 inch diameter by 0.062 inch thick copper sheet covered with the test coating. The monitor is a 1.25 inch square by 0.005 inch thick beryllium copper sheet coated with a black paint (carbon black, Cat-O-Lac black, Parson's

black).* In the center of the back face of each sample a copper-constantan thermocouple junction is imbedded. Four fiberglas strings are attached to each sample for mounting purposes. Figure 2 shows the position of the samples when mounted in the frames. Four screw-down washers on each frame secure the sample strings. The two thermocouple wires pass through Delrin-insulated† holes in the frames so that they do not tangle during the rotation of the sample.

The frames were painted with Cat-O-Lac black paint in order to minimize reflections from the frames to the samples. Cat-O-Lac black has a solar absorptance of 0.95. The trapezoid design was the result of an attempt to minimize diffuse radiation emitted from the frames to the samples. If the frame surfaces emit according to Lambert's law it can be shown that the rate of radiation from a trapezoid-shaped monitor frame to the test sample will be approximately 10% less than the rate of radiation from a rectangular-shaped monitor frame to the test sample. Since the sample frame is also trapezoid in shape, the 10% reduction in radiation rate also applies when considering the rate of radiation from the sample frame to the monitor sample.

The assembled apparatus as it appears in the high vacuum chamber is sketched in Figure 3. The axis of the shafts was established by

*The different shapes of the monitor and test sample were chosen for convenience.

†Delrin: An acetyl resin compound of low thermal conductivity and excellent strength; available through E. I. Dupont de Nemours and Company, Wilmington, Delaware.

dropping a plumb line from the top plate of the shroud. The shafts are aluminum for greater thermal conductivity as compared to stainless steel, and they are in thermal contact with the liquid-nitrogen-cooled shroud at its top plate and its table. A Delrin insulator was inserted in the aluminum shaft below the shroud table to eliminate heat conduction from the shroud table through the base table to the base plate, since the shroud is thermally insulated from the base plate as shown. Bearings at the shroud table and the base table facilitate the rotation of the lower frame. A chain and sprocket arrangement with a 4 to 1 ratio couples the main shaft with the rotary feed-through shaft. A 180° turn of the rotary feed-through shaft then produces a 45° turn of the sample.

## Calibration of Sample Holder

In order to know the angular displacement of the sample with respect to the incident light as the rotary feed-through shaft is turned, an optical method of calibrating the system using the principle of perpendicularity was devised. A sensitive measurement of perpendicularity of a reflecting object to an incident parallel beam of light may be made by causing the incident and reflected slit beam to coincide.

A 2.5 inch diameter lucite disk with three plane, mirrored faces was used as the reflection optics. As shown in Figure 4, face 1 was machined parallel to the screw hole center line (plane of frame) so that when the disk is mounted in the sample frame, face 1 is parallel to the

plane of the frame. Face 2 is then 30° and face 3 is 60° from the plane of the frame. As the shaft connected to the sample frame is rotated, one face comes into perpendicularity with an incident beam at 0°, 30°, and 60°.

An 8-inch collimator was modified to allow light from a high intensity lamp to enter a 1/32 inch diameter hole in a diaphragm located at the focal point of its objective. The objective beam was reduced from a 2.5 inch diameter beam to a 1/16 inch by 1/2 inch vertical slit beam to eliminate the paraxial rays of the objective. The collimator was fastened to an adjustable table and was carefully leveled in the vertical and horizontal planes.

An initial step in the actual calibration involved establishing an axis perpendicular to the vacuum chamber port window. This involves movement of the collimator table until the beam from the objective slit is reflected by the port window back on itself. At this point the collimator and its table are fixed in position. The lucite disk is then positioned in the rotary frame and is placed in the chamber. As the frame is rotated, face 1 becomes perpendicular to the collimator beam. When this position is located, the 0° angular displacement of the sample frame is determined. Face 2 and face 3, the 30° and 60° faces respectively, are brought into normality by further rotation of the frame. These three angular positions were marked during the first calibration of the system on a brass blank dial located around the rotary feed-through

handle. A dividing head instrument was used to determine the true angular distance between the three positions. Angle marks from 0° to 90° were then engraved on the disk relative to the three reference marks.

The final phase of the alignment involves positioning the carbon arc light source so that its collimated beam lies along the already established axis of the collimator beam and the reflected beam from the lucite disk. A diaphragm with a small pinhole was placed in front of the arc crater, and a second diaphragm with a pinhole was placed over the collimator lens of the arc. A small beam of light through the pinholes was established by placing a light source in the arc crater. Movement of the entire arc lamp unit then allowed this beam to pass entirely through the collimator and onto the port of the bell jar, at which point the two beam axes coincided.

## OPERATING PROCEDURE FOR OBTAINING THE SOLAR ABSORPTANCE $\bar{a}(\theta)$

### The Thermal Vacuum Technique for Determining $\bar{a}/\bar{e}$

The high vacuum chamber employed for these tests operates at a base pressure of $2 \times 10^{-7}$ torr. A liquid-nitrogen-cooled cylindrical shroud, located inside the bell jar, provides a cold wall, high absorptance surrounding for the samples. The solar simulator, a high intensity

arc lamp, is collimated with an 8-1/2 inch diameter quartz lens.* Temperatures of the test sample, the monitor sample, and other points within the chamber are monitored by a multipoint recorder. Sample temperatures have also been monitored by using a manually balanced potentiometer bridge.

Thermal vacuum methods measure the $\bar{a}/\bar{e}$ or $\bar{e}$ of a satellite coating by the temperature or the rate of temperature change of the materials. The type of thermal measurement employed for this experiment is an equilibrium temperature measurement of $\bar{a}/\bar{e}$ in which the sample is heated by the solar simulator until equilibrium temperature is reached. This measurement as opposed to an alternate method, the transient thermal vacuum technique, eliminates the error involved in extrapolating the curve of $dT/dt$ vs $\sigma T^4$ to $dT/dt = 0$ in order to calculate the hemispherical emittance of the sample.

After the samples are mounted in their frames and placed in the vacuum system, the chamber is pumped down to $2 \times 10^{-7}$ torr and the walls of the shroud are cooled to approximately -193°C. The samples are then heated by the solar simulator until the thermocouple sensors indicate that both the monitor and the test sample have reached their equilibrium temperatures. The samples are maintained at this temperature for as long as 15-20 minutes to insure against a long time variation in the temperature of the test sample. This procedure is followed for

*The intensity of incident illumination of the collimated carbon arc beam varies ±3% across the face of the 5" diameter port of the bell jar.

each angle of incidence to which the test sample is turned. The black monitor sample, which comes to equilibrium faster than the test sample because of its small time constant, has a twofold purpose:

1. Because of its small time constant, the monitor sample reveals drift in arc intensity "before the test sample sees the drift." The intensity can then be readjusted by repositioning the negative carbon in the arc lamp.
2. The equilibrium temperature of the monitor sample determines the absolute intensity of the arc.

The rate of change of thermal energy with time of a sample is equal to the power absorbed by the sample of projected area $A_p$, plus the power P absorbed from incident thermal radiation of the walls of the shroud and the quartz window, minus the thermal power radiated from the total surface area $A_s$ of the sample. The heat balance equation is therefore:

$$mc \frac{dT}{dt} = A_p \bar{a} I + P - A_s \bar{e} \sigma T^4 , \qquad (1)$$

where

m = mass of the sample,

I = total radiant power per unit area of the solar simulator,

c = specific heat of the sample substrate,

T = temperature,

$\sigma$ = Stefan-Boltzman constant,

$\bar{a}$ = average solar absorptance of the sample's illuminated area (this depends on the direction of incident illumination),

$\bar{e}$ = average thermal emittance of the sample,

t = time.

At thermal equilibrium the change in temperature with time for the sample is zero; Equation 1 becomes

$$0 = A_p \bar{a} I + P - A_s \bar{e} \sigma T^4 \quad . \tag{2}$$

Assuming that P, the power absorbed from incident thermal radiation from the walls of the vacuum chamber is zero, Equation 2 becomes:

$$0 = A_p \bar{a} I - A_s \bar{e} \sigma T^4 ,$$

from which

$$\frac{\bar{a}}{\bar{e}} = \frac{A_s}{A_p} \cdot \frac{\sigma T^4}{I} \quad . \tag{3}$$

A complete description of thermal vacuum methods for measuring the absorptance and emittance properties of spacecraft materials and a description of the equipment employed for these measurements at the Goddard Space Flight Center is given by Fussell, Triolo, and Henninger.[1]

## Calculation of $\bar{a}(\theta)$

The $\bar{a}/\bar{e}$ of a coating is a function of the angle of incidence of the beam. Hence, Equation 3 is written

$$\frac{\bar{a}(\theta)}{\bar{e}(\theta)} = \left(\frac{A_s}{A_p} \cdot \frac{\sigma T^4}{I}\right)_{\theta, s} = \frac{\bar{a}(\theta)}{\bar{e}} \tag{4}$$

where the subscript $(\theta, s)$ implies the angle of incidence of the test sample. The $\bar{a}(\theta)/\bar{e}(\theta)$ is assumed equal to $\bar{a}(\theta)/\bar{e}$ : that is, we assume the $\bar{e}$ of a sample is not temperature dependent $\left[\bar{e}(\theta) = \bar{e}\right]$.* This is not a valid assumption; however, at the present time the error incorporated in an emittance measurement using a thermal vacuum technique would completely obscure the small correction for the change in $\bar{e}$ with temperature. For normal incidence Equation 4 is written

$$\frac{\bar{a}(0°)}{\bar{e}(0°)} = \left(\frac{A_s}{A_p} \cdot \frac{\sigma T^4}{I}\right)_{0°, s} = \frac{\bar{a}(0°)}{\bar{e}} \tag{5}$$

Dividing Equation 4 by Equation 5 gives

$$\frac{\bar{a}(\theta)}{\bar{a}(0°)} = \left(\frac{A_{p,0°}}{A_{p,\theta}} \cdot \frac{T_\theta^4 - I_{0°}}{T_{0°}^4 - I_\theta}\right)_s . \tag{6}$$

A similar set of equations may be written for the monitor sample. However, since the monitor is not rotated from one test to the next, the equation that corresponds to Equation 6 is expressed as

*The emittance of a sample varies slightly with temperature within the operational range of +100° C to −50° C since the equilibrium temperature of the sample is different at each angle of incidence setting. The emittance is actually an explicit function of temperature and in this experiment the emittance becomes an implicit function of angle; i.e. $\bar{e} = \bar{e}\,(T(\theta))$. The $\bar{e}(\theta)$ above is equivalant to $\bar{e}\,(T(\theta))$ and is assumed equal to $\bar{e}$.

$$1 = \left( \frac{T_\theta^4}{T_{0^\circ}^4} \cdot \frac{I_{0^\circ}}{I_\theta} \right)_m \quad , \tag{7}$$

where the subscripts $0^\circ$ and $\theta$ refer to the values at the times when the test sample is at the angles $0^\circ$ and $\theta$, and m stands for monitor. Equation 7 gives the intensity ratio

$$\frac{I_{0^\circ}}{I_\theta} = \left( \frac{T_{0^\circ}^4}{T_\theta^4} \right)_m \quad . \tag{8}$$

Substituting Equation 8 into Equation 6 gives

$$\frac{\bar{a}(\theta)}{\bar{a}(0^\circ)} = \left( \frac{A_{p,0^\circ}}{A_{p,\theta}} \frac{T_\theta^4}{T_{0^\circ}^4} \right)_s \left( \frac{T_{0^\circ}^4}{T_\theta^4} \right)_m \tag{9}$$

The projected area of the test sample $A_{p,\theta}$ in Equation 9 changes as the sample is rotated to different angles:

$$A_{p,\theta} = A_{p,s} \cos\theta + A_{p,e} \sin\theta \tag{9a}$$

where $A_{p,s} \cos\theta$ is the projected area of the sample face at an angle $\theta$, and $A_{p,e} \sin\theta$ is the projected area of the sample edge at an angle $\theta$.

The final step in calculating $\bar{a}(\theta)$, the directional solar absorptance, is to measure $\bar{a}(0^\circ)$ by an independent method. For this measurement an optical method is used which employs a Beckman DK-2 spectrophotometer with an integrating sphere reflectance attachment. Thus:

$$\frac{\bar{a}(\theta)}{\bar{a}(0^\circ)} \cdot \bar{a}(0^\circ)_{optical} = \bar{a}(\theta) \quad . \tag{10}$$

Future measurements will incorporate the change in emittance with temperature of each test coating. A modified Dymec 2010C Data Acquisition System will be used for recording sample temperatures along with calibrated thermocouples from -200°C to +100°C. These modifications will increase the accuracy of the temperature readings from ±0.7% to ±0.008%.

## EXPERIMENTAL RESULTS

The solar absorptances of some selected coatings as a function of angle from the normal are presented in Figures 5 through 9. Each graph is a plot of $\bar{a}(\theta)$ vs $\theta$, where $\bar{a}(\theta)$ has been calculated according to the discussion in the previous section. In most cases, measurements have been terminated at $\theta = 75°$ because of the large percent of the illuminated edge area of the test sample at these larger angles. Measurements beyond 75° have been tried with some coatings, however, the results indicate that errors due to edge area were present.

Values of the directional solar absorptance of a coating as presented in Figures 5-9 are essential for calculating the amount of radiation absorbed by a spherical vehicle. Drummeter and Fowler[2] have shown that by appropriately integrating over the surface of a hemisphere one obtains the following expression for the hemispherical solar absorptance:

$$\bar{a}_H = 2 \int_0^{\pi/2} \bar{a}(\theta) \sin\theta \cos\theta \, d\theta. \qquad (11)$$

The evaporated aluminum data presented in Figure 5 will be used to demonstrate the calculation of $\bar{a}_H$. The extrapolated section of the curve in Figure 5 was used. It can be shown that whatever the true curve is at these points, the extrapolated curve in all probable cases is no more than 3% in error.

Figure 10 shows the plot of the integrand of Equation 11 vs $\theta$ from $\theta = 0°$ to $\theta = \pi/2$ for the evaporated aluminum data. Mechanical integration of the curve yields the value:

$$\bar{a}_H = 0.0926$$

which is within 2% of the value stated by Hass.*

It is interesting to note that the value stated by Hass was obtained theoretically by using the Fresnel equations[3] of the exact form. For a particular opaque coating with optical constants $n(\lambda)$ and $k(\lambda)$, the hemispherical solar reflectance $\bar{r}_H$ of the coating is obtained by integrating the Fresnel equations over the solar spectrum and over a hemispherical surface. The hemispherical solar absorptance is then $1 - \bar{r}_H = \bar{a}_H$.

*Private communication with G. Hass, USAERDL, Fort Belvoir, Va.

## MAJOR ERRORS AFFECTING THE ACCURACY OF $\bar{a}(\theta)$

The errors affecting the accuracy of the $\bar{a}(\theta)$ values have been separated into two groups: those which limit the accuracy of the angular setting of the sample, and those involved in the thermal equilibrium experiment.

Errors in the angular setting of the test sample are random and evolve during the calibration process. First, there exists an error in the accuracy with which the reflected beam from the lucite disk can be superimposed on the incident beam. This calculated error is $\Delta\theta_1 = \pm 0.040°$. Second, there is an error $\Delta\theta_2$ when the arc lamp is aligned for normal incidence. A calculation shows that $\Delta\theta_2 = \pm 0.193°$. A third error is involved in marking the 0°, 30°, and 60° reference marks and the subsequent engraving of the brass dial. The maximum estimated error is $\Delta\theta_3 = \pm 0.250°$.

The total random error $\Delta\theta$, combining $\Delta\theta_1$, $\Delta\theta_2$, and $\Delta\theta_3$ is $\Delta\theta = \pm 0.318°$. Since the projected area of the sample $A_p$ is a function of $\sin\theta$ and $\cos\theta$, the $\Delta\theta$ error produces an angular dependent error in $A_p$. A calculation shows that for normal incidence the percentage error in the $A_s/A_p$ ratio is ±0.25%; at 75° the percentage error becomes ±3%.

The present data for $\bar{a}(\theta)$ has been obtained by assuming that both the sample face and the sample edge are at the angle $\theta$. The error in the $\bar{a}(\theta)$ for the evaporated aluminum data at 75° due to this assumption is approximately +10%. This error arises in Equation 9a. The $A_{p,s} \cos \theta$ term is related to the absorptance of the sample face at an angle $\theta$ whereas the $A_{p,e} \sin \theta$ term is related to the absorptance of the sample edge at an angle $\pi/2 - \theta$. A heat balance equation which accounts for the different absorptance of the sample face and sample edge is:

$$\bar{a}(\theta)\, A_{p,s} \cos \theta + \bar{a}(\pi/2-\theta)\, A_{p,e} \sin \theta = \left(\frac{A_s \bar{e} \sigma T^4}{I}\right)_{\theta,s}$$

The major error which limits the accuracy of the thermal equilibrium experiment is the measurement of the equilibrium temperature of the samples. In the present system, the accuracy of the temperature reading is ±0.7%. With more accurately calibrated thermocouple wires this error should be reduced to ±0.008%. This is a random error and cannot be corrected.

A possible source of error due to the variation of thermal emittance with temperature of the sample coating and the variation of specific heat with temperature of the sample substrate does exist but is small compared with the temperature measurement error (see the section on the "Calculation of $\bar{a}(\theta)$").

A second source of possible error (systematic), neglected in this experiment is reflected radiation on the sample from the back of the cylindrical shroud.

The total percentage error in the $\bar{a}(\theta)$ values determined in this experiment is expressed as

$$\Delta\bar{a}(\theta) = \left[(0.7)^2 + (1.5)^2 + \left(\Delta\frac{A_s}{A_p}\right)_\theta^2\right]^{1/2},$$

where

0.7 = percentage error in equilibrium temperature measurements,

1.5 = percentage error in $\bar{a}(0°)$ measurement using the Beckman DK-2 Spectrophotometer for evaporated aluminum (the error is dependent on the reflectance of the material),

$\left(\Delta\frac{A_s}{A_p}\right)_\theta$ = percentage error in $A_s/A_p$ ratio which is dependent on $\theta$.

The difference in spectral distribution between the solar simulator and the sun is a source of error for which no correction was made in these measurements. This error is difficult to estimate, but it can be seen that since $\bar{a}(\theta)$ is calculated by taking the ratio of:

$$\frac{\bar{a}(\theta)}{\bar{a}(0°)}\left(\bar{a}(0°)_{optical}\right),$$

where $\bar{a}(0°)_{optical}$ is appropriately weighted for the solar spectrum, less of an error due to the miss-match is present than if only the $\bar{a}/\bar{e}$ of the coating were measured.

## CONCLUSIONS

An acceptably accurate method for measuring the solar absorptance of satellite coatings as a function of angle of incidence has been established. This method involves a precise rotational apparatus and an already established reliable measurement of the $\bar{a}/\bar{e}$ of satellite coatings by using a thermal vacuum equilibrium technique.

Directional solar absorptances for five different selected coatings have been measured. The data obtained from these measurements can be used to calculate the hemispherical and cylindrical absorptance of typical spacecraft materials. The hemispherical absorptance for evaporated aluminum as measured by this experiment compares closely with a theoretical value. The continued close agreement of experimental values with theory for single layered samples will justify possible future measurements of complicated layered samples, and their acceptance as being reliable.

## FUTURE IMPROVEMENTS AND MODIFICATIONS

Improvements to the present experiment which will be incorporated in future modifications are the following:

1. A direct method for rotating the sample frame which eliminates gear backlash, gear slippage, and tedious calibration. Such a method would incorporate a Decitrak Shaft-Position Encoder* coupled to the rotating shaft of the sample frame. This encoder has a resolution of 0.1°.

2. The off-center positioning of the sample frame in order to minimize any error due to refocusing on the sample of arc light incident on the rear wall of the shroud.

3. An "edgeless" test sample so that errors in the $\bar{a}(\theta)$ values due to edge effects at large angles of incidence will be minimized. A plano-convex sample has been suggested. Such a sample will make measurements up to 85° feasible.

## REFERENCES

1. Fussell, W. B., Triolo, J. J., and Henninger, J. H., "A Dynamic Thermal Vacuum Technique for Measuring the Solar Absorptance and Thermal Emittance of Spacecraft Coatings," NASA TN D-1716, (March 1963).

*Decitrak, Model #DE-1-40-B-2-A-CW, made by Theata Instrument Corporation, Saddle Brook, New Jersey.

2. Drummeter, L. F., Jr., and Fowler, W. B., "Emittance and Absorptance of Pure Aluminum," NRL itr 7360-412, Ser: 10543, U.S. Naval Res. Lab., (November 1959).

3. Heavens, O. S., *Optical Properties of Thin Solid Films* (Academic Press Inc., New York, 1955), Chapter 4.

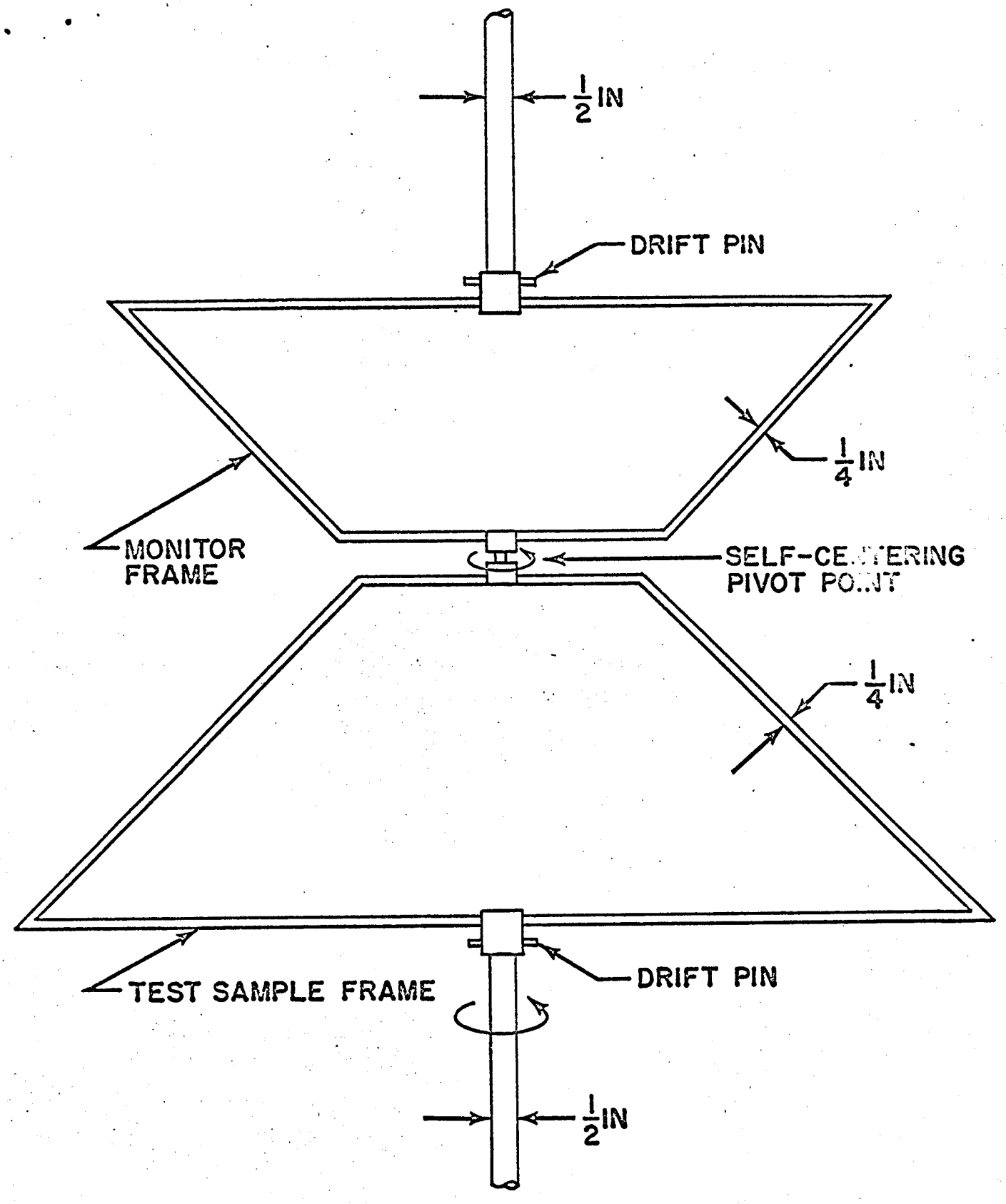


FIGURE 1.—CONNECTION AND ROTATION DETAIL OF FRAMES

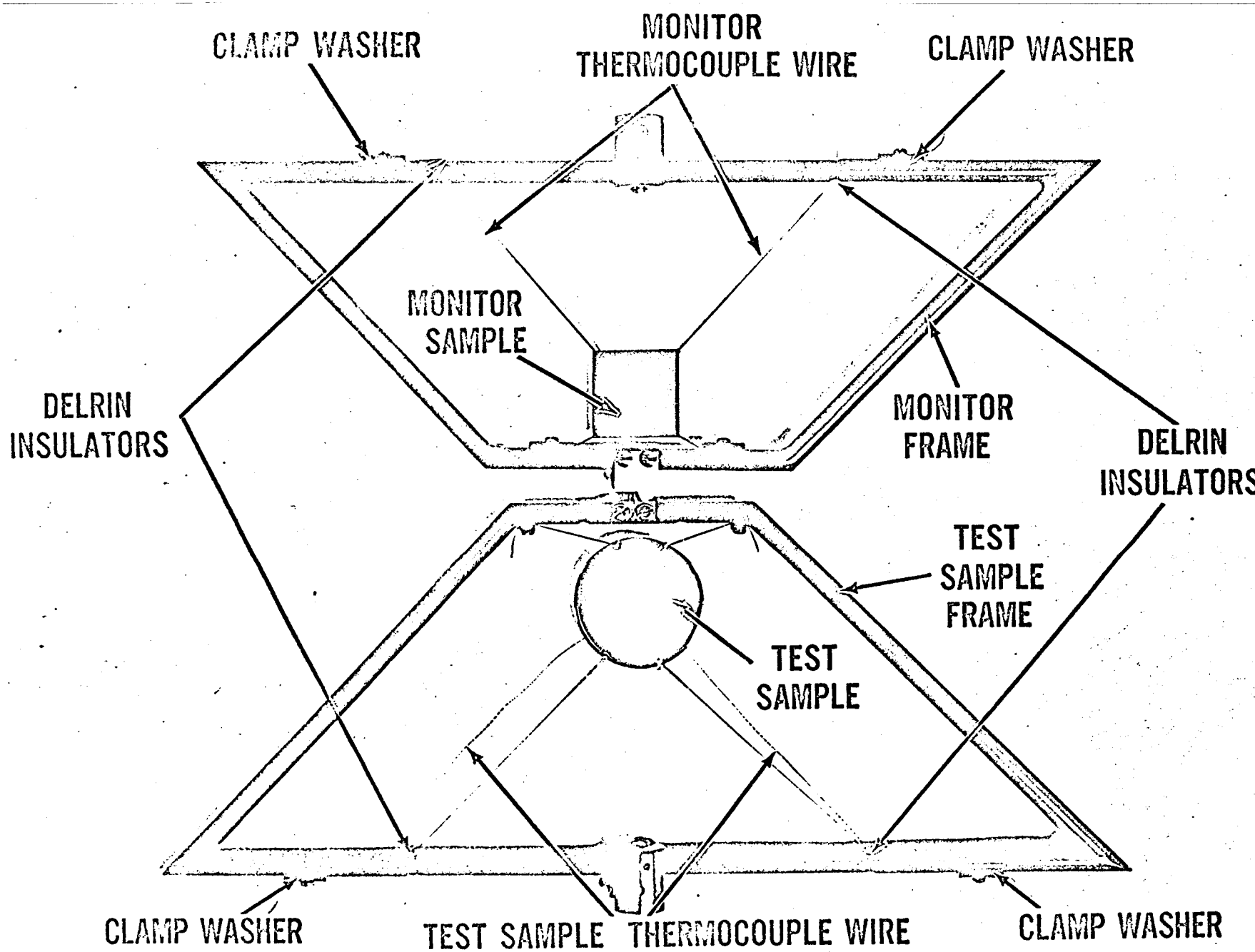


FIGURE 2. The Monitor and Test Sample Frames with Samples Mounted in "Testing Position"

NASA C-64- 2599

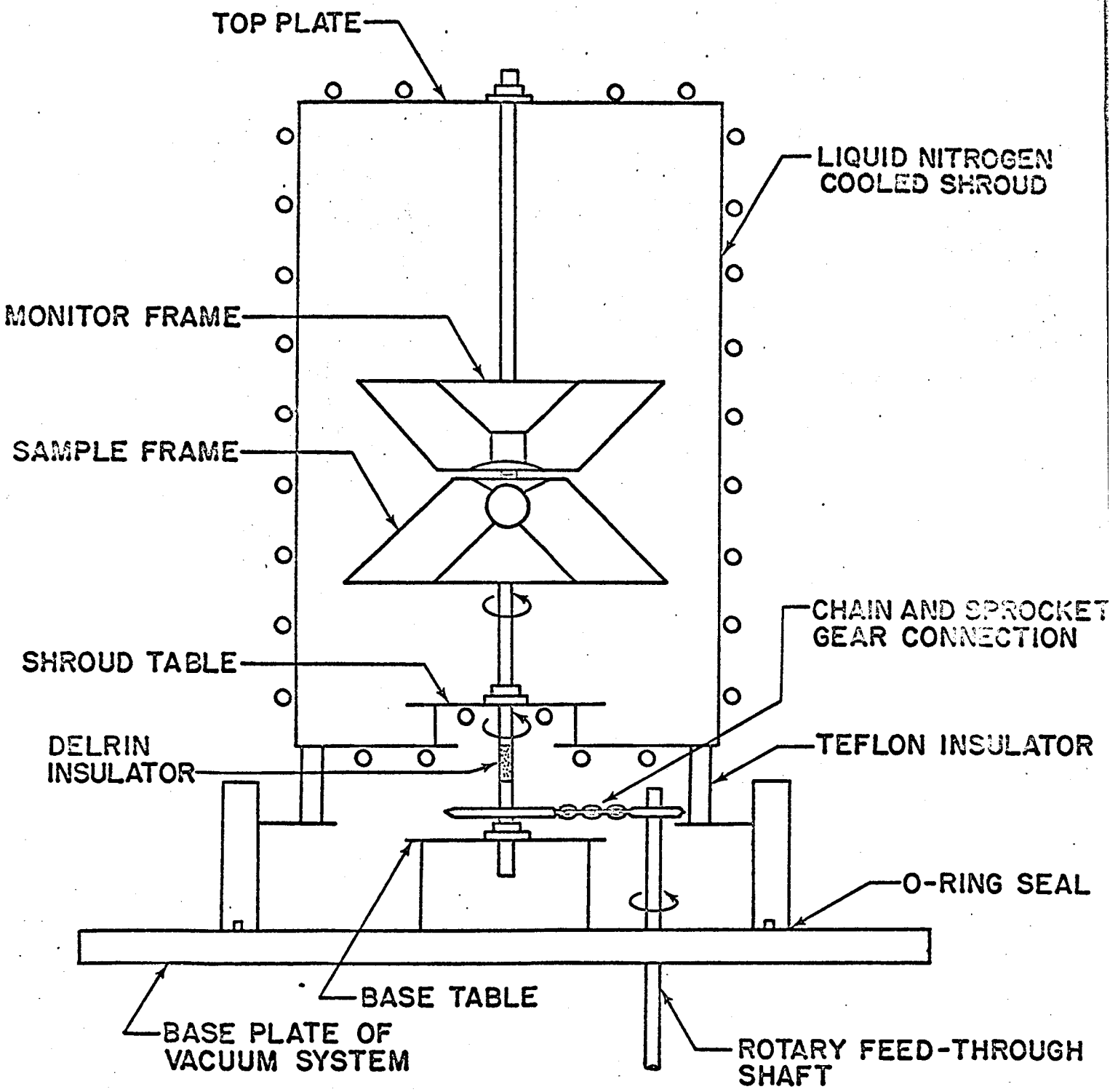


FIGURE 3- CROSS SECTION OF THE SHROUD WITH ROTATIONAL APPARATUS INSTALLED

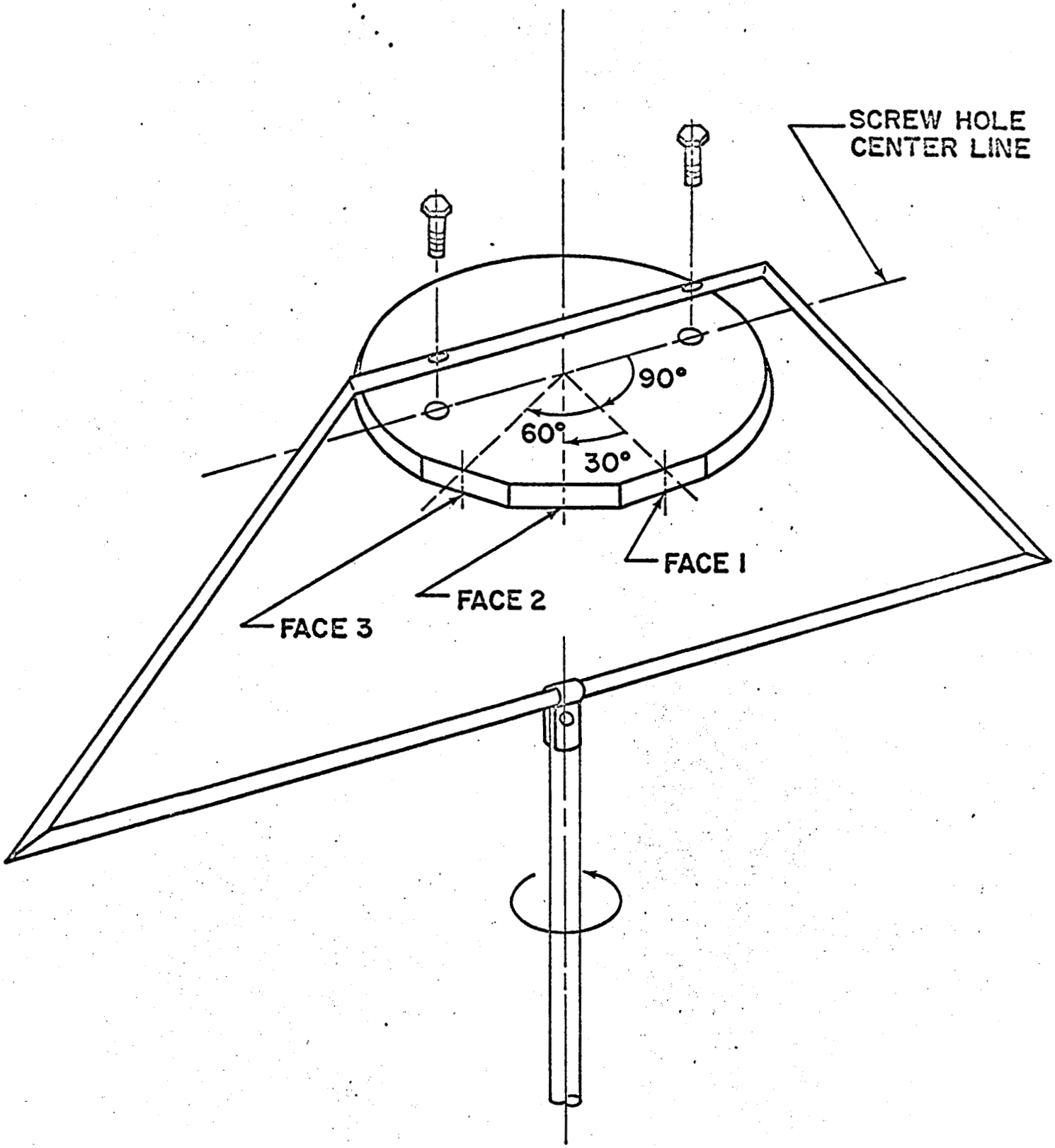


FIGURE 4.- LUCITE REFLECTING DISK MOUNTED IN ROTATING FRAME

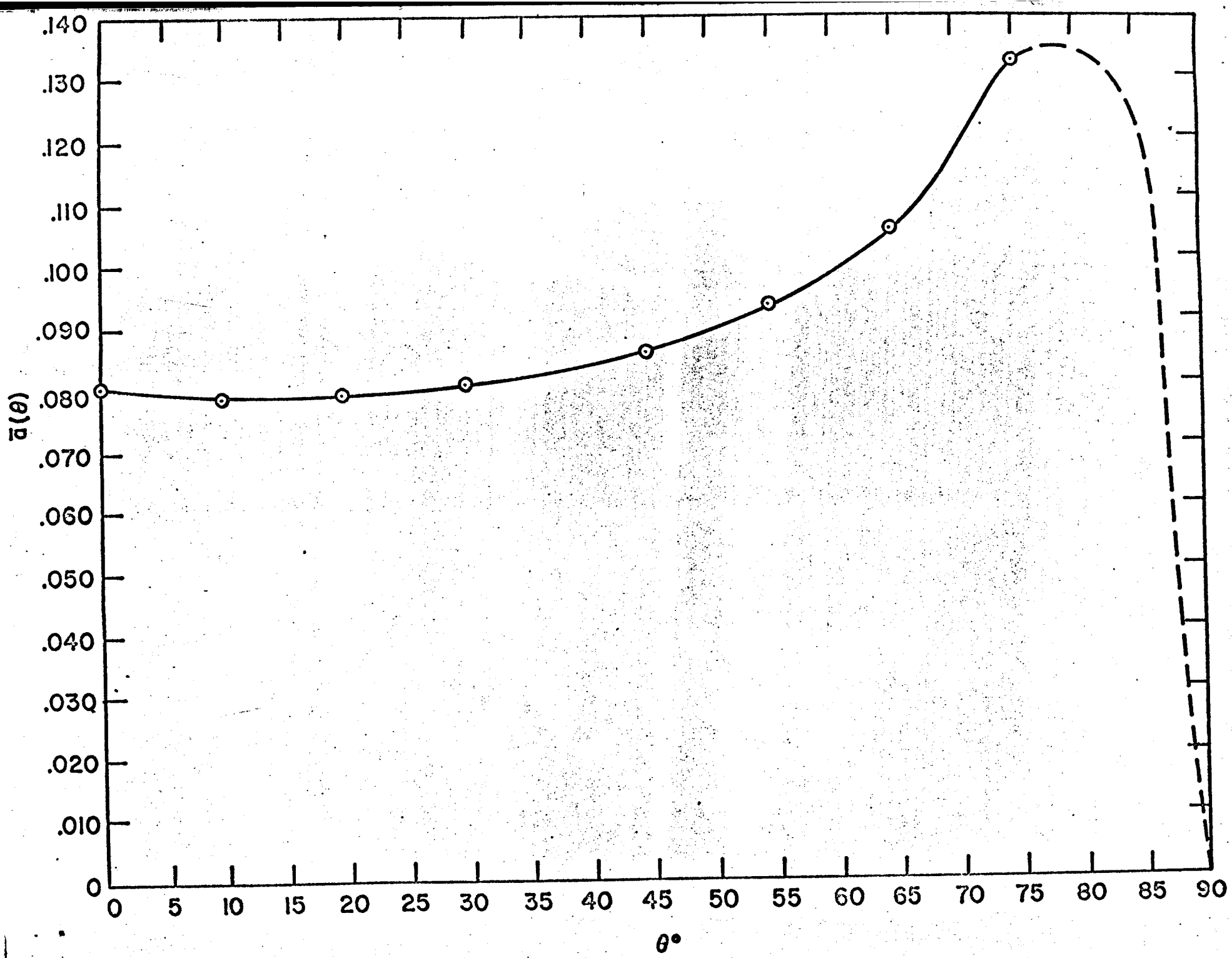


FIGURE 5 – DIRECTIONAL SOLAR ABSO[illegible]TANCE OF EVAPORATED ALUMINUM
(AVERAGE OF T[illegible] OF DATA)

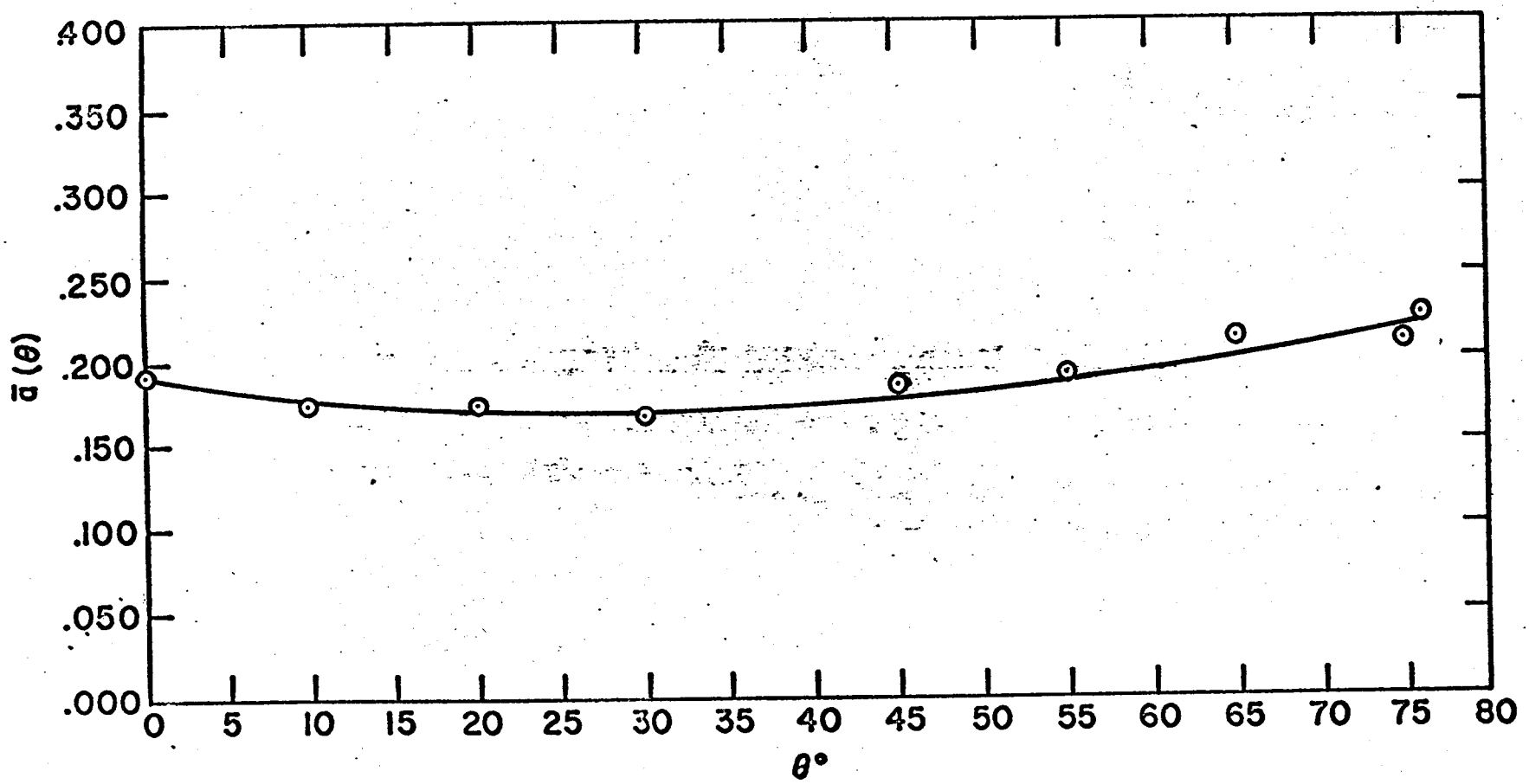


FIGURE 6 - DIRECTIONAL SOLAR ABSORPTANCE OF EVAPORATED GOLD (SINGLE SET OF DATA)

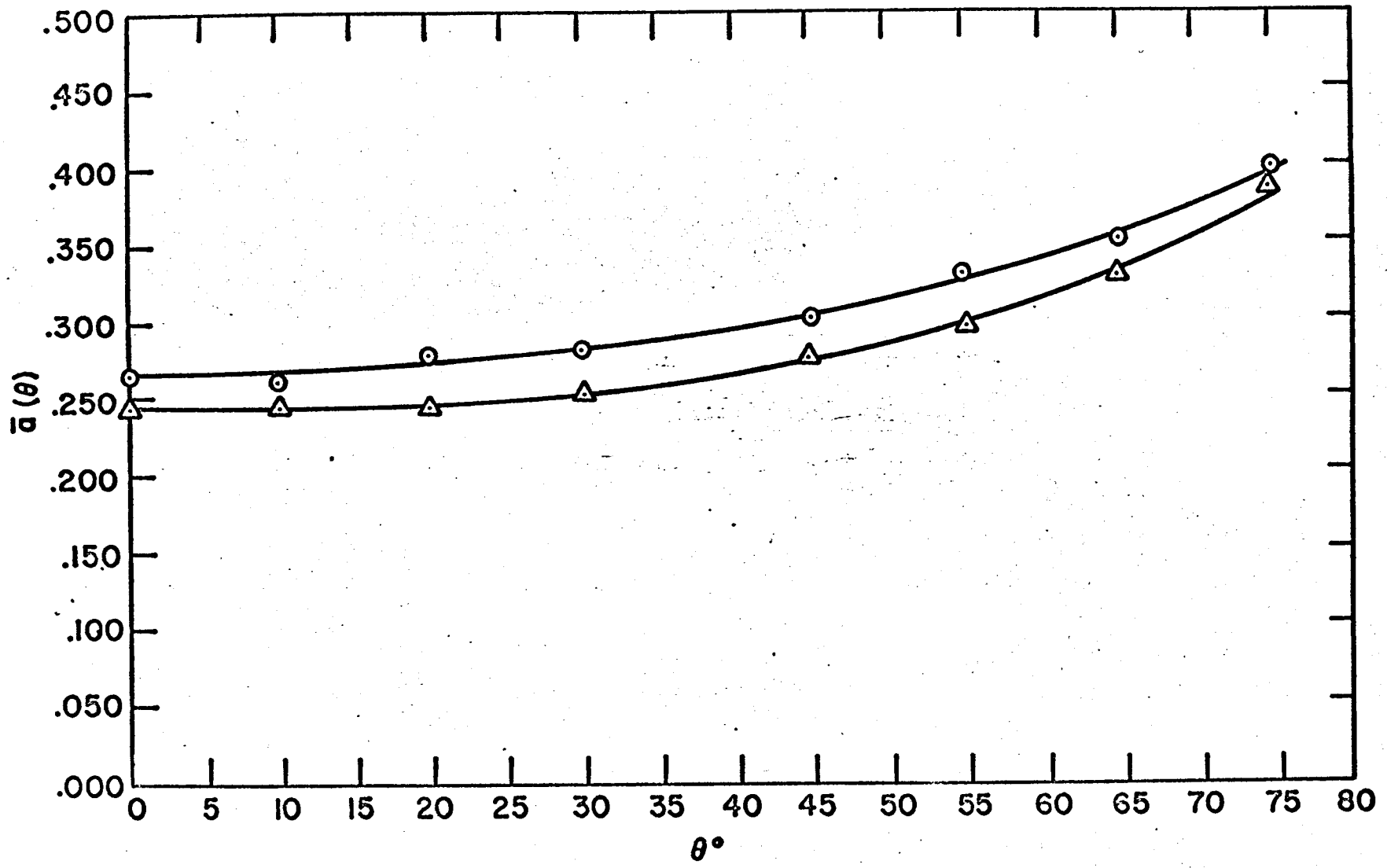


FIGURE 7- DIRECTIONAL SOLAR ABSORPTANCE
OF ALUMINUM LEAFING PAINT (TWO SETS OF DATA)

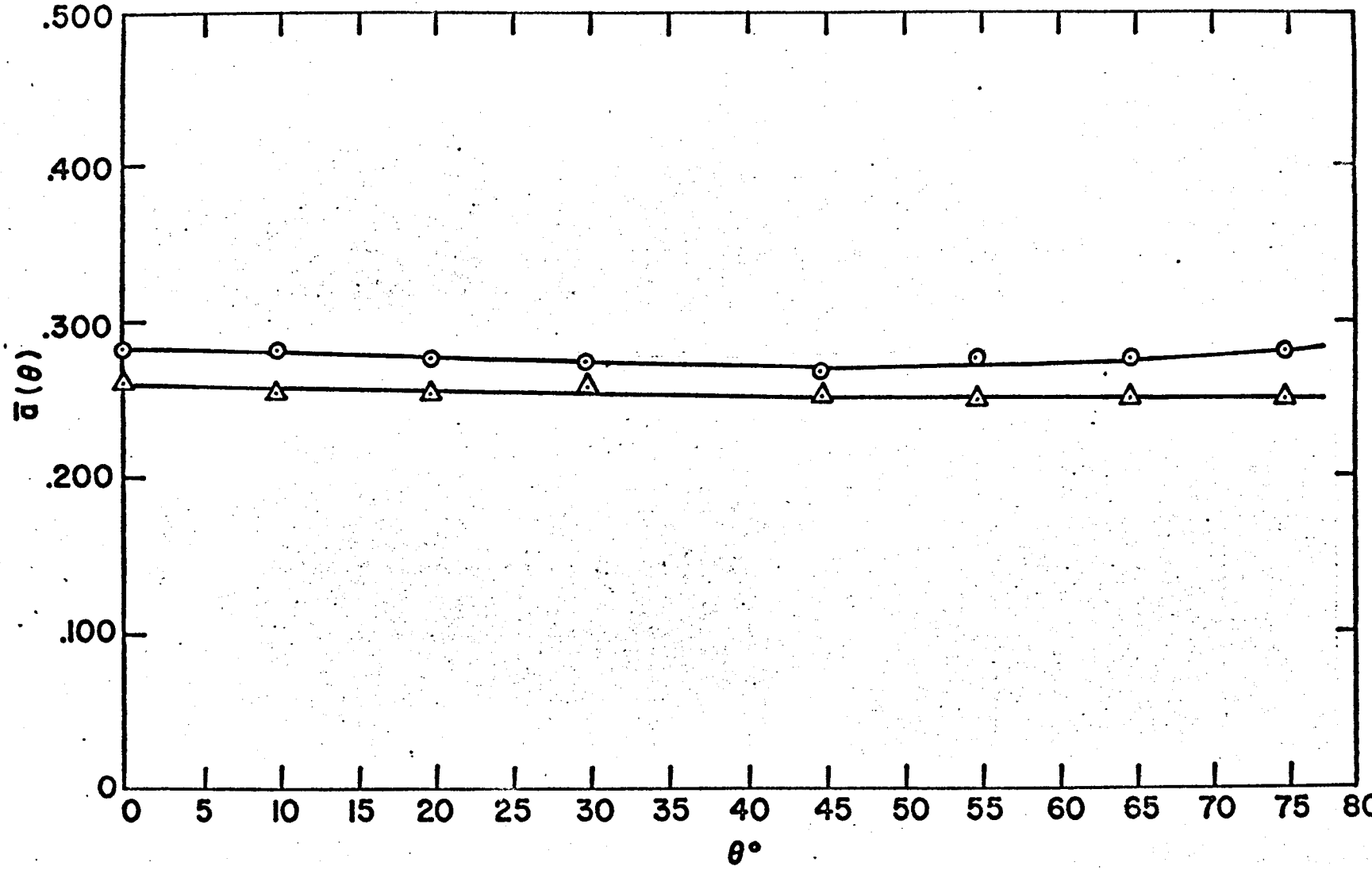


FIGURE 8 – DIRECTIONAL SOLAR ABSORPTANCE OF ZINC SULFIDE PAINT (TWO SETS OF DATA)

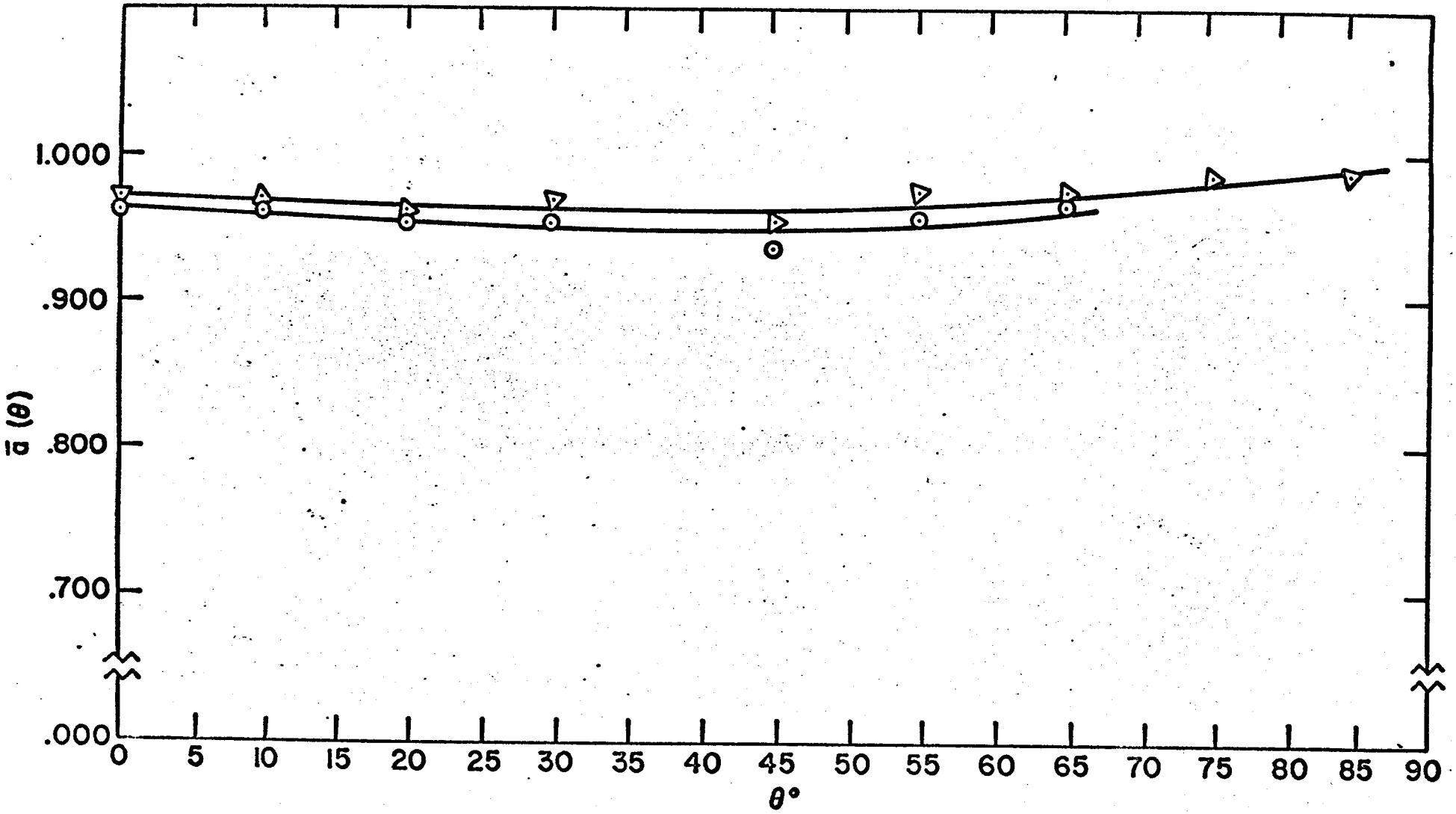


FIGURE 9. DIRECTIONAL SOLAR ABSORPTANCE OF PARSON'S BLACK PAINT (TWO SETS OF DATA)

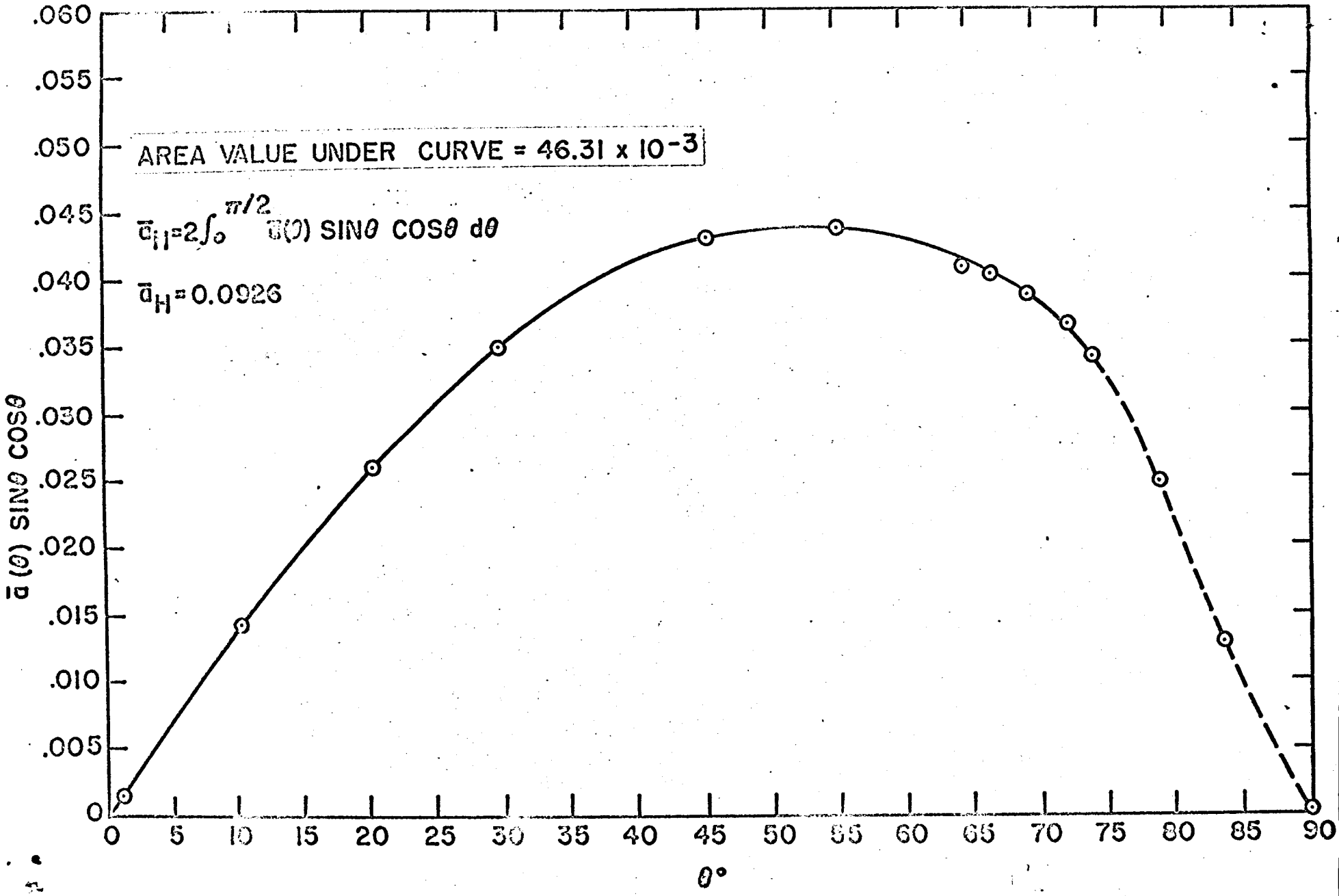


FIGURE 10. PLOT OF INTEGRAND OF EQUATION II FOR EVAPORATED ALUMINUM DATA (FIGURE 5)

# LIST OF FIGURES